

# Supporting Information

## Synthesis and Electrocatalytic Performance of Atomically Ordered Nickel Carbide (Ni<sub>3</sub>C) Nanoparticles

Nor A. Fadil,<sup>†,‡,§</sup> Govindachetty Saravanan,<sup>†</sup> Gubbala V. Ramesh,<sup>\*,†</sup> Futoshi  
Matsumoto,<sup>§§</sup> Hideki Yoshikawa,<sup>†</sup> Shigenori Ueda,<sup>†</sup> Toyokazu Tanabe,<sup>†</sup> Toru  
Hara,<sup>†</sup> Shinsuke Ishihara,<sup>†</sup> Hideyuki Murakami,<sup>†</sup> Kazuhiko Noda<sup>‡</sup>, Katsuhiko  
Ariga,<sup>†,⊥</sup> and Hideki Abe<sup>\*,†,¶</sup>

<sup>†</sup> National Institute for Materials Science, 1-1 Namiki, Tsukuba, Ibaraki 305-0044, Japan

<sup>§</sup> Universiti Teknologi Malaysia, 81310 Skudai, Johor Bahru, Johor, Malaysia

<sup>‡</sup> CSIR-National Environmental Engineering Research Institute (CSIR-NEERI),  
Environmental Materials Division, Nehru Marg, Nagpur 440020, India.

<sup>§§</sup> Kanagawa University, 3-27 Rokkakubashi, Yokohama, Kanagawa 221-8686, Japan

<sup>††</sup> Synchrotron X-ray Station at SPring-8, National Institute for Materials Science,

<sup>†</sup> MANA, National Institute for Materials Science (NIMS), 1-1 Namiki, Tsukuba, Ibaraki  
305-0044, Japan

<sup>⊥</sup> CREST, Japan Science and Technology Agency (JST), 1-1 Namiki, Tsukuba, Ibaraki 305-  
0044, Japan

<sup>¶</sup> PRESTO, Japan Science and Technology Agency (JST), 4-1-8 Honcho Kawaguchi,  
Saitama 332-0012, Japan

ABE.Hideki@nims.go.jp, GUBBALA.Venkataramesh@nims.go.jp

## Table of contents

1. Materials
2. Methods
  - 2.1 Synthesis of Ni-Cp clusters
  - 2.2 Synthesis of Ni<sub>3</sub>C nanoparticles (Nps)
  - 2.3 Synthesis of pure Ni Nps
  - 2.4 Powder X-ray diffractometry
  - 2.5 Hard X-ray photoemission spectroscopy
  - 2.6 Transmission electron microscopy
  - 2.7 Fourier-transform infrared spectroscopy
  - 2.8 Electrochemistry
3. Characterization
  - 3.1 Ni-Cp clusters
  - 3.2 Ni<sub>3</sub>C Nps
  - 3.3 Pure Ni Nps
4. Additional electrochemical data
  - 4.1 NaBH<sub>4</sub> oxidation over Au Nps
  - 4.2 Methanol oxidation
5. References

## 1. Materials

Organometallic Ni precursors were used as purchased from Aldrich: nickel cyclopentadienyl ( $\text{NiCp}_2$ , 99 % in purity) and nickel acetylacetonate ( $\text{Ni}(\text{acac})_2$ , 95 % in purity). Sodium (Nihon Soda Co.) and Naphthalene (Kishida Chemicals) were used also as purchased. Tetrahydrofuran (THF, 99.5 %), toluene (96 %) and methanol (99.8 %) were received from Kishida Chemicals. THF and toluene were distilled prior to use under vacuum to remove oxygen and moisture. Methanol was de-aired by bubbling with dry Ar for 30 min. The chemical reagents and solvents were always treated under a dry Ar atmosphere. A wire of pure Ni (1 mm in diameter, 99.9 %) was purchased from Nilaco as a reference for photoemission spectroscopy. Pure Au Nps (average particle size < 100 nm) were used as purchased from Aldrich for electrochemical tests.

## 2. Methods

### 2.1 Synthesis of Ni-Cp clusters

An aliquot of 1.5 mmol of a reducing agent, sodium naphthalide ( $\text{NaNaph}$ ), was first prepared in a dry Ar atmosphere. An aliquot of 1.5 mmol each of sodium chunk (0.0345 g) and Naphthalene (0.1923 g) were stirred in 50 ml of THF overnight in a tri-neck flask, one of which port was capped with a rubber septum. The sodium chunk and Naphthalene were fully dissolved in THF to form a dark-green solution of  $\text{NaNaph}$ .

An aliquot of 0.375 mmol of  $\text{NiCp}_2$  (0.0708 g) was dissolved in 10 ml of distilled THF in a dry Ar atmosphere to yield a green solution. The solution was transferred into a syringe and quickly injected into the  $\text{NaNaph}$  solution through the septum of the tri-neck flask. The solution changed in color from dark green to dark brown upon injection and became black after a several seconds. The solution was stirred for one more hour to complete the reaction. THF was then removed through distillation to leave a dark brown precipitate. The precipitate was washed with toluene and methanol in sequence to remove byproducts. At each washing process, the precipitate was dispersed in the solvent through sonication for 2 min and separated from the supernatant by centrifugation at 6000 rpm. The final product was thoroughly dried by evacuation at room temperature to yield a black, air-sensitive powder consisting of Ni-Cp clusters (see 3.1).

## 2.2 Synthesis of Ni<sub>3</sub>C nanoparticles (Nps)

The final product obtained by chemical reduction of NiCp<sub>2</sub>, Ni-Cp clusters, was subsequently annealed without exposed to air. The black powder was wrapped in a Ta foil in a dry Ar atmosphere and sealed in a quartz ampoule together with an oxygen-getter, Zr foil. The quartz ampoule was evacuated down to 20 Pa and backfilled with dry Ar gas up to 50 kPa. The quartz ampoule was then heated overnight at 200 °C in a tubular furnace. The synthesized Ni<sub>3</sub>C Nps was a black, air-stable powder (see 3.2).

## 2.3 Synthesis of pure Ni Nps

An aliquot of 1.5 mmol each of sodium chunk (0.0345 g) and Naphthalene (0.1923 g) were dissolved in 50 ml of THF, contained in a tri-neck flask having a septum on one of the ports, to develop a THF solution of NaNaph (see 2.1). An aliquot of 0.375 mmol of Ni(acac)<sub>2</sub> (0.0963 g) was dissolved in 10 ml of distilled THF in a dry Ar atmosphere to yield a pale-green solution. The solution was transferred into a syringe and injected into the NaNaph solution through the septum. The solution changed in color from dark green to dark brown upon injection. The solution was stirred for one more hour to complete the reaction. THF was then removed by distillation to leave a dark brown precipitate. The precipitate was washed with toluene and methanol in sequence to remove byproducts. At each washing step, the precipitate was dispersed in the solvent through sonication for 2 min and separated by centrifugation at 6000 rpm. The precipitate was thoroughly dried by evacuation at room temperature to yield a black, air-stable powder comprising pure Ni Nps (see 3.3).

## 2.4 Powder X-ray diffractometry

Powder X-ray diffractometry (*p*XRD) was performed using CuK $\alpha$  radiation (RIGAKU RINT 2000;  $\lambda = 0.1548$  nm) with an increment of 0.02 degrees in a range of diffraction angles from 30 to 80 degrees. A single-crystalline Si plate was used as a sample holder to minimize backgrounds. Samples for *p*XRD were prepared in an inert atmosphere to prevent possible oxidation. First, thick grease (Apiezon-H) was squeezed in a circle on the sample holder. Sample powders were placed in the center of the circle and covered with a polyimide film (Kapton, 0.3 mm in thickness) such that the powders were always in a confined space formed by the film, grease and the holder.

## 2.5 Hard X-ray photoemission spectroscopy

Hard X-ray photoemission spectroscopy (HX-PES) was performed at the undulator beamline BL15XU of SPring-8. The excitation photon energy was set to 5.95 keV. Sample powders were first dispersed in methanol or acetone in air and dropped onto Nb-doped, single-crystalline substrates of SrTiO<sub>3</sub>. The samples were thoroughly dried in air and transferred into an ultra-high-vacuum (UHV) chamber attached to an electron spectrometer (VG Scienta R4000HKE). The binding energy of photoelectrons was referenced to the Fermi energy of an Au film that was electrically contacted to the samples.

## 2.6 Transmission electron microscopy

An ultra-high-vacuum scanning transmission electron microscope (UHV-TEM; TECNAI G<sup>2</sup>) was used to examine the morphology, particle size and atomic arrangements of the synthesized Nps. Another UHV-TEM equipped with a CCD camera (JEM-2010F with Gatan Orius 200D) was used to perform transmission electron diffraction (TED). Samples for UHV-TEM were prepared by dropping methanol suspensions of the Nps onto commercial TEM grids coated with collodion films. Prior to UHV-TEM observation, the samples were thoroughly dried by evacuation at room temperature.

## 2.7 Fourier-transform infrared spectroscopy (FTIR)

An FTIR spectrometer (Perkin-Elmer, Spectrum GX-R) was used to examine the chemical state of organic ligands in Ni-Cp clusters as well as NiCp<sub>2</sub>. The spectrometer was equipped with a MIRTGS detector and operated in a single-beam absorbance mode at 1 cm<sup>-1</sup> resolution. The FTIR data were averaged over 32 scans to reduce noises. Samples for FTIR were prepared in an inert atmosphere. Apiezon-H grease was squeezed in a circle on a sample holder (single-crystalline KBr; 20x30x4 mm<sup>3</sup>). Sample powders were placed in the center of the circle and covered with another KBr holder such that the powders were always in a confined space formed by grease and the pair of holders.

## 2.8 Electrochemistry

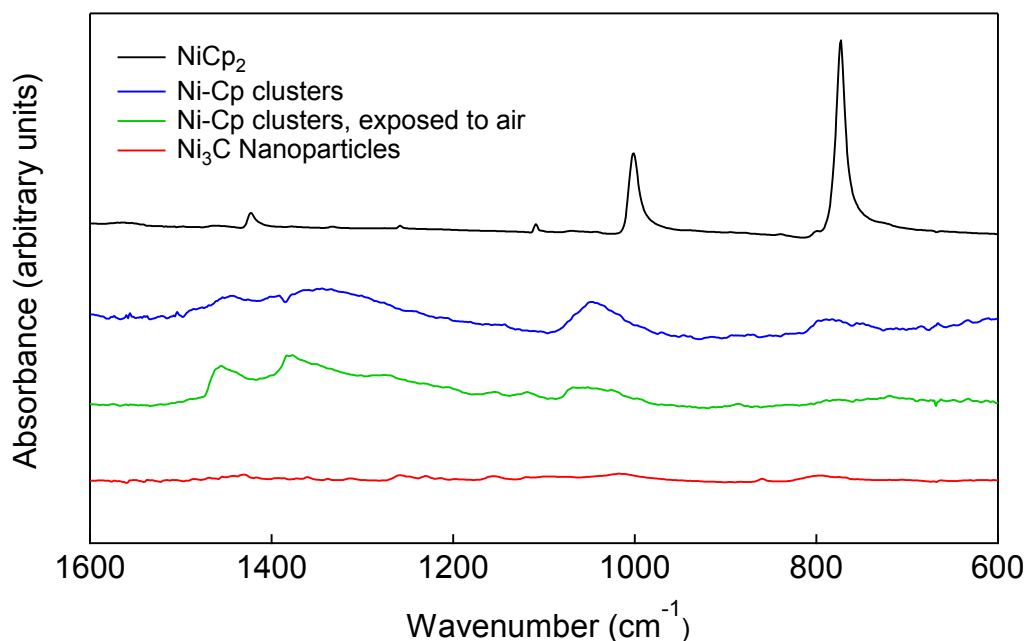
A glassy carbon (GC) electrode (5 mm in diameter, Hokuto Denko) was polished prior to use with a #2000 emery paper, which was followed by 1- and 0.06 mm alumina powders over a Milli-Q-water-wetted microcloth (Buhler). The GC electrode was then sonicated in Milli-Q water for 10 min and finally rinsed with Milli-Q water. An aliquot of 1.75 mg of Ni<sub>3</sub>C-, pure Ni- or Au Nps was suspended in a mixture of 1745  $\mu$ L of distilled water, 439  $\mu$ L of isopropyl alcohol, and 9  $\mu$ L of a 5 % w/w lower aliphatic alcohols-water solution of Nafion (EW: 1100, Aldrich). After sonication for 15 min, the suspension was dropped onto the GC electrode and dried in air. The GC electrode was coated with 13.7  $\mu$ g each of Ni<sub>3</sub>C-, Ni- or Au Nps.

Cyclic voltammetric (CV) or Linear-scan voltammetric (LV) measurements were performed using a computer-controlled electrochemical system (HSV-100, Hokuto Denko) in a three-electrode, two-compartment electrochemical cell (main compartment volume = 50 mL). A Pt wire was used as the counter electrode, and an Ag/AgCl electrode, consisting of potassium chloride-saturated silver/silver chloride (Ag/AgCl, KCl-sat.), was used as the reference. The GC electrodes were rotated at 2000 rpm during the electrochemical measurements. All voltammograms were measured at room temperature (23 $\pm$ 1  $^{\circ}$ C) and at a potential sweep rate of 10 mVs<sup>-1</sup>.

Before performing measurements on the electro-oxidation of MeOH (Wako) and NaBH<sub>4</sub> (Wako), background currents were first measured in de-aerated aqueous solutions of 0.5 M KOH (Wako) for MeOH and 2 M NaOH (Wako) for NaBH<sub>4</sub>, respectively. Electro-oxidation of MeOH and NaBH<sub>4</sub> was examined in aqueous solutions of 0.5 M MeOH/0.5 M KOH and 0.2 M NaBH<sub>4</sub>/2 M NaOH, respectively. The solutions were de-aerated with purified nitrogen gas over 10 min prior to measurements. An O<sub>2</sub>-saturated solution was prepared for electrochemical measurements on the oxygen reduction reaction (ORR) by bubbling Milli-Q water with a purified O<sub>2</sub> gas (> 99.99995 vol.%). Finally, stability of the Ni<sub>3</sub>C Nps catalyst was tested in aqueous solution of 0.1 M NaBH<sub>4</sub> and 2M NaOH by repeating 25 cycles of CV from -1.1 V to 0.0 V (vs. Ag/AgCl) at a potential sweep rate of 10 mVs<sup>-1</sup>.

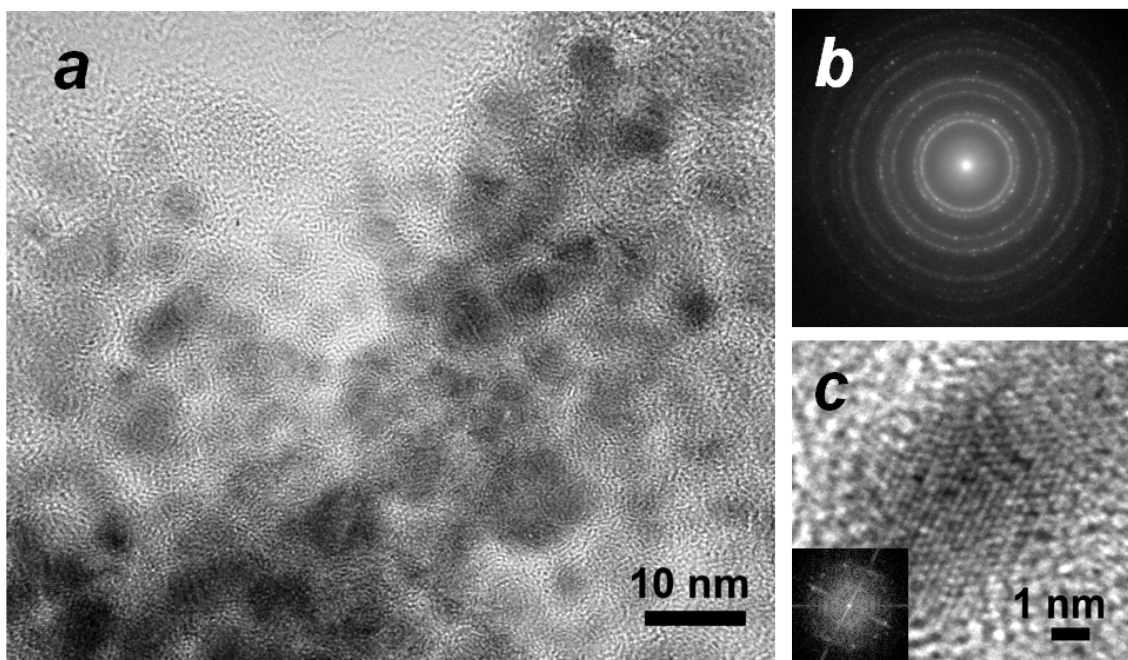
### 3. Characterization

#### 3.1 Ni-Cp clusters



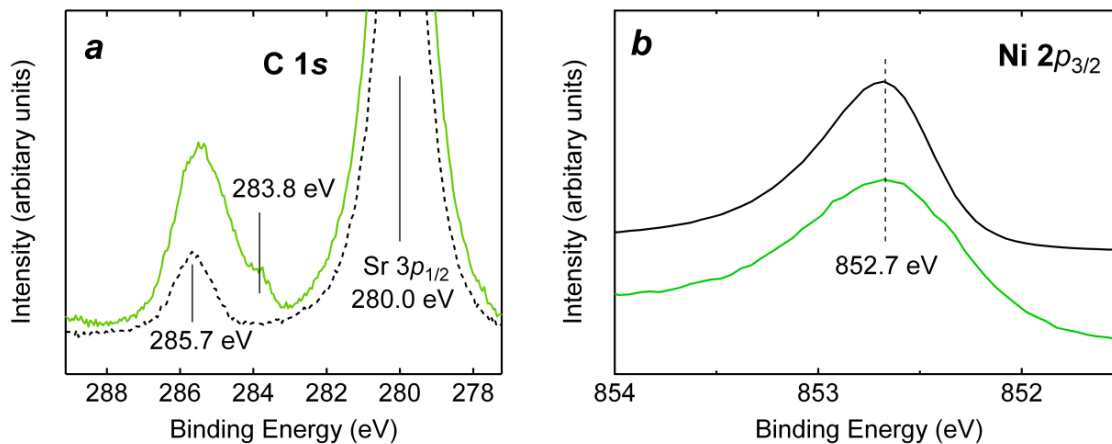
**Figure S1:** FTIR spectra of NiCp<sub>2</sub> (black), Ni-Cp clusters (blue), Ni-Cp clusters exposed to air (green) and Ni<sub>3</sub>C Nps (red).

Figure S1 shows the FTIR spectra of NiCp<sub>2</sub>, Ni-Cp clusters, air-exposed Ni-Cp clusters and Ni<sub>3</sub>C Nps. Three peaks are observed on the FTIR profile for NiCp<sub>2</sub> at 750, 1000 and 1420 cm<sup>-1</sup>, corresponding to the C-H out-of-plane bending, C-H in-plane-bending and C=C stretching of the ligand Cp molecule, respectively (black curve).<sup>1</sup> All the FTIR peaks corresponding to the vibration of Cp became broad and weak when NiCp<sub>2</sub> was reduced to form Ni-Cp clusters (blue curve). The C-H vibrational modes of Ni-Cp clusters had larger wavenumbers (C-H out-of-plane bending and in-plane-bending at 780 and 1050 cm<sup>-1</sup>, respectively) than those of NiCp<sub>2</sub>. When exposed to air, Ni-Cp clusters were partly decomposed to form nickel carbides likely due to exothermal oxidation, resulting in diminished C-H vibrational peaks (green curve). All the C-H vibrational peaks disappeared when Ni-Cp clusters were fully converted to Ni<sub>3</sub>C Nps by heating in vacuum at 200 °C (red curve).



**Figure S2:** (a) Bright-field TEM image, (b) electron diffraction image and (c) high-resolution TEM image of the air-exposed Ni-Cp clusters.

Figure S2a presents a bright-field UHV-TEM image of the air-exposed Ni-Cp clusters showing agglomerated Nps. Transmission electron diffraction (TED) showed that the Nps were very similar in crystal structure to FCC-type Ni (Figure S2b). Disordered lattice fringes showed that the Nps were atomically disordered (Figure S2c). Indeed, Fourier-transformation of Figure S2c resulted in multiple spots, reflecting the atomic disorder in this nanoparticle (see the inset of Figure S2c).



**Figure S3:** (a) HX-PES profiles in the C 1s and Sr 3p<sub>1/2</sub> regions for the air-exposed Ni-Cp clusters (green curve) and the SrTiO<sub>3</sub> substrate (black broken curve). (b) HX-PES profiles in the Ni 2p<sub>3/2</sub> region for bulk Ni (black) and the air-exposed Ni-Cp clusters (green).

Figure S3 shows the HX-PES spectra in the C 1s- and Ni 2p<sub>3/2</sub> regions for the air-exposed Ni-Cp clusters. The C 1s photoemission peak from surface contamination was observed at 285.7±0.2 eV on both the air-exposed Ni-Cp clusters and the substrate (Figure S3a). An additional shoulder was recognized at 283.8±0.2 eV on the air-exposed Ni-Cp clusters, which was close to the C 1s binding energy for Ni<sub>3</sub>C, 283.7±0.2 eV (see Figure 2e of the main text). The Ni 2p<sub>3/2</sub> photoemission peak of the air-exposed Ni-Cp clusters was dispersed in binding energy but consistent with that of bulk Ni, showing Ni atoms in the air-exposed Ni-Cp clusters were similar in chemical environment to metal Ni (Figure S3b). The air-exposed Ni-Cp clusters were, as expected from FTIR (Figure S1) and UHV-TEM (Figure S2), contained atomically disordered nickel carbide that presumably contained less carbon than Ni<sub>3</sub>C.

### 3.2 Ni<sub>3</sub>C Nps

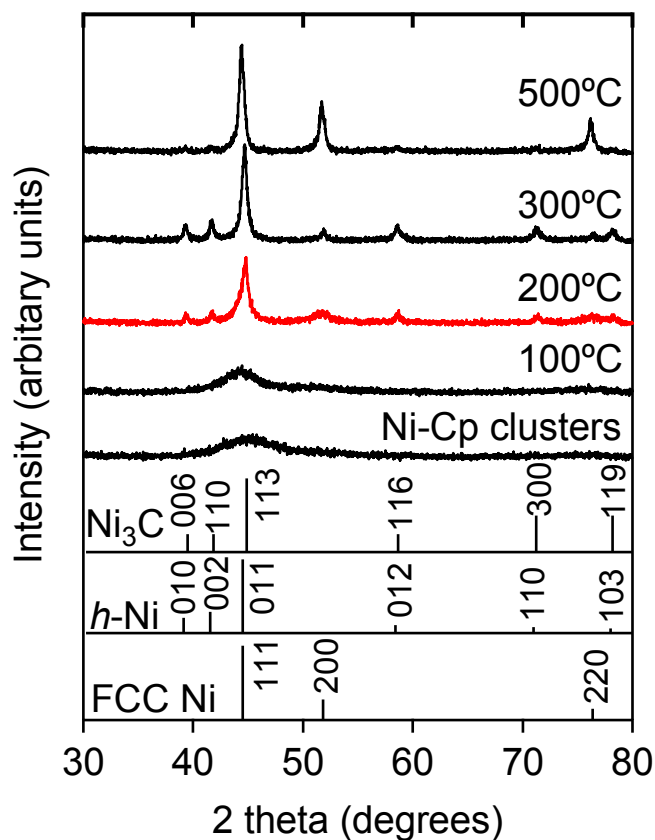


**Figure S4:** *p*XRD profiles for Ni-Cp clusters and the products obtained by annealing Ni-Cp clusters in vacuum at different temperatures. Simulated *p*XRD peaks for the FCC-type Ni (*Fmm*,  $a = 0.3524$  nm), hcp-type Ni (*h*-Ni;  $a = 0.265$ - $0.267$  nm,  $c = 0.433$ - $0.435$  nm)<sup>2</sup>, and rhombohedral Ni<sub>3</sub>C (*Rc*;  $a = 0.455$  nm,  $c = 1.29$  nm) are indicated by solid markers.

Figure S4 presents *p*XRD profiles for Ni-Cp clusters and the products obtained by annealing Ni-Cp clusters at different temperatures. The 006, 110, 116 and 300 reflections of the rhombohedral Ni<sub>3</sub>C phase were clearly visible at 200 and 300 °C, but disappeared when the annealing temperature was 500 °C, as the result of thermal decomposition of Ni<sub>3</sub>C. The Ni<sub>3</sub>C phase, formed at 200 °C as Nps (S5, see Figure 2 of the main text), was thermally stable up to 300 °C.

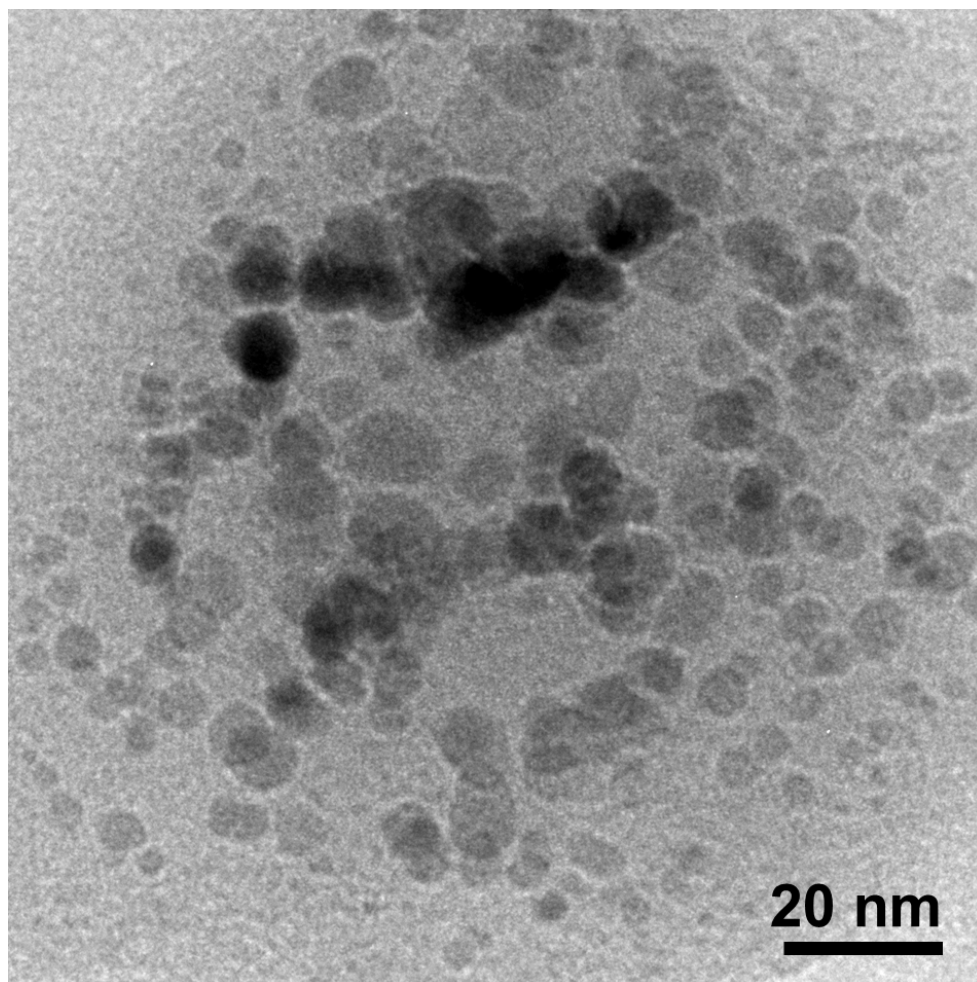


**Figure S5:** Bright-field TEM image of Ni<sub>3</sub>C Nps for a large area.

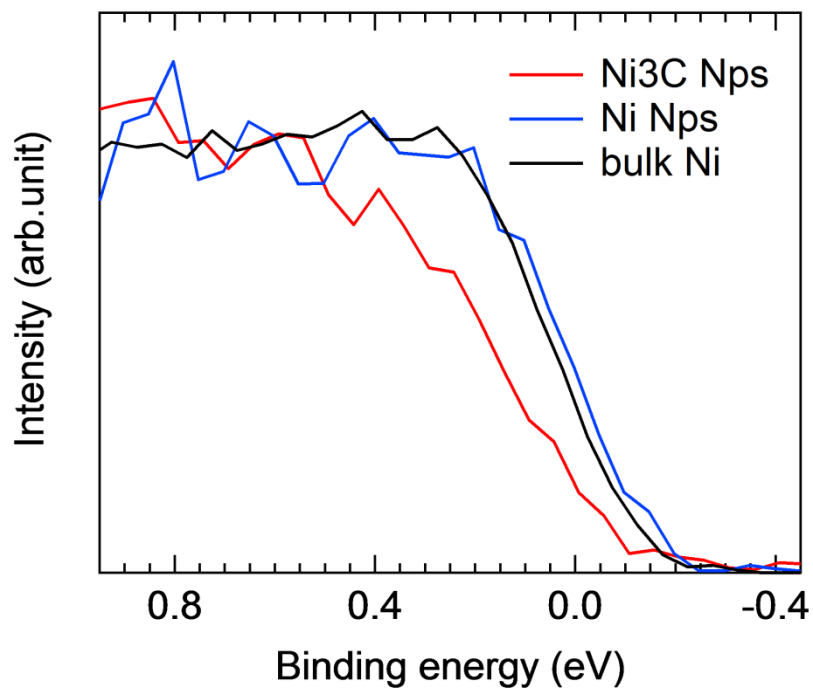


**Figure S6:** HX-PES profiles in the valence region for the Ni<sub>3</sub>C Nps (red), Ni Nps (blue) and bulk Ni (black).

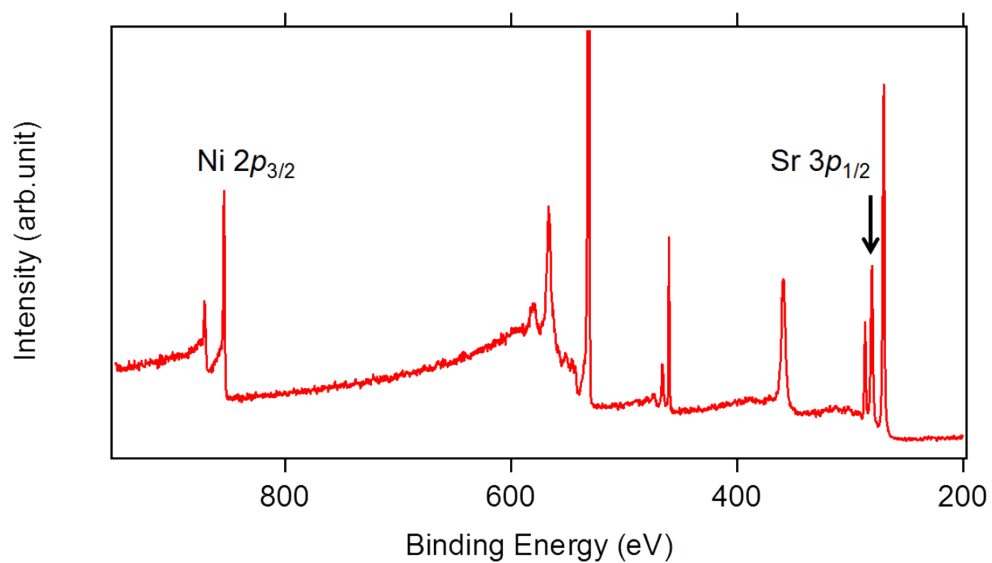


**Figure S7:** HX-PES profile for the Ni<sub>3</sub>C Nps, acquired over a wide range of binding energy.

Figure S7 shows a wide-range HX-PES data of the Ni<sub>3</sub>C Nps. The intensities of the Ni 2p<sub>3/2</sub>- and C 1s emissions are evaluated as 2.05±0.2 and 0.0411±0.0004 (arbitrary units), respectively. The mole ratio of Ni to C is calculated as Ni : C = 1.0 : 0.31±0.03 by the following formula, using the reported photoemission cross sections for the Ni 2p<sub>3/2</sub>- and C 1s emissions at a photon energy of 6 keV, 3.0480 × 10<sup>3</sup> barn and 1.9998 × 10<sup>2</sup> barn, respectively ("Theoretical photoionization cross sections from 1 to 1500 keV", James H. Scofield, (1973), Lawrence Livermore Laboratory report UCRL-51326):

$$\text{Ni} : \text{C} = (2.05/(3.0480 \times 10^3)) : (0.0411/(1.9998 \times 10^2)) = 1.0 : 0.31.$$

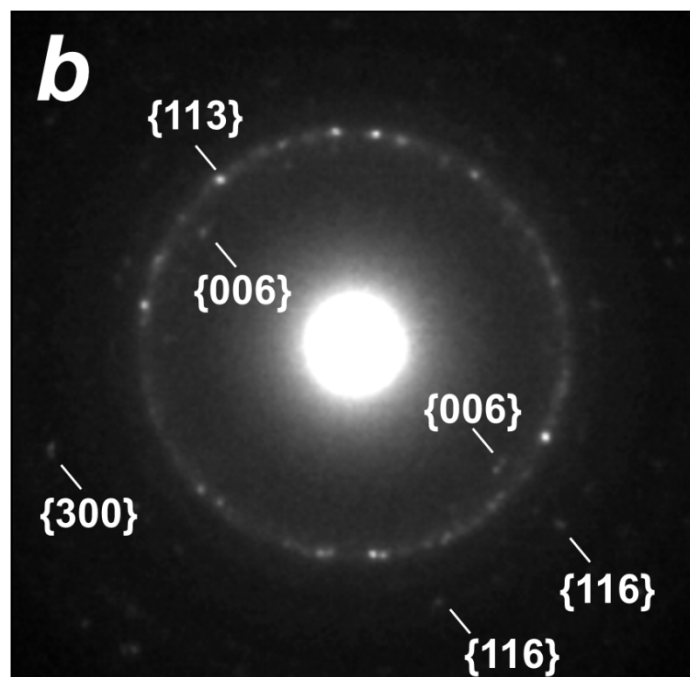
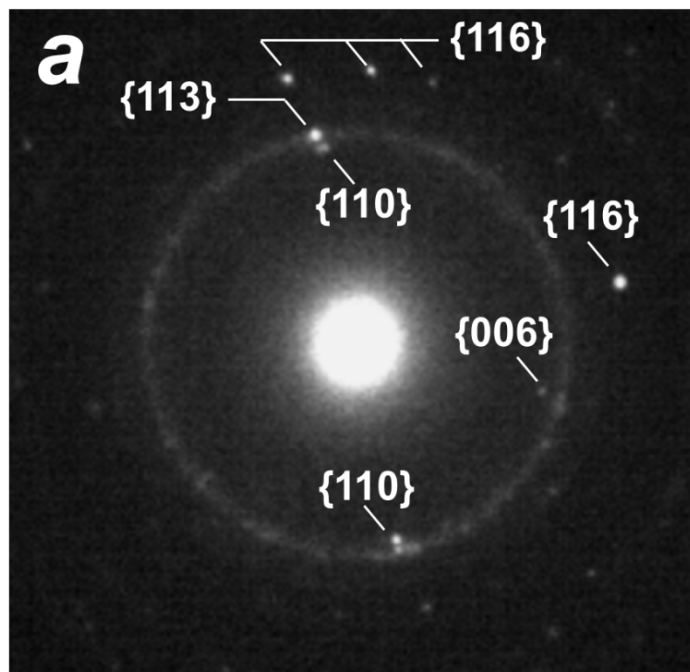


**Figure S8:** Transmission electron diffraction (TED) patterns for the prepared Ni<sub>3</sub>C Nps (a) and the Ni<sub>3</sub>C Nps which experienced repeated electrochemical cycles in an aqueous solution of NaOH and NaBH<sub>4</sub> (b).

Figure S8a shows that the Ni<sub>3</sub>C NPs before the catalysis, as expected from powder X-ray diffraction (pXRD), exhibit a TED pattern corresponding to rhombic Ni<sub>3</sub>C (*Rc*; *a* = 0.455 nm, *c* = 1.29 nm). There are recognized the Ni<sub>3</sub>C {006} reflections of which *d*-value, 0.2153 nm, is larger than the largest *d*-value of Ni, 0.2035 nm, of the {111} reflections (S8a). In addition to the {006} reflections, there are recognized the other reflections including Ni<sub>3</sub>C {110}, {116} and {113}. Importantly, the Ni<sub>3</sub>C Nps, which have experienced the repeated electrochemical cycles in the working condition, still exhibit a TED pattern corresponding to the rhombic Ni<sub>3</sub>C phase: the large-*d*-value {006} reflections, {116}- and {300} reflections (S 8b). The Ni<sub>3</sub>C Nps retain their chemical composition and crystal structure even when they are subjected to the repeated operation of fuel cells.

### 3.3 pure Ni Nps

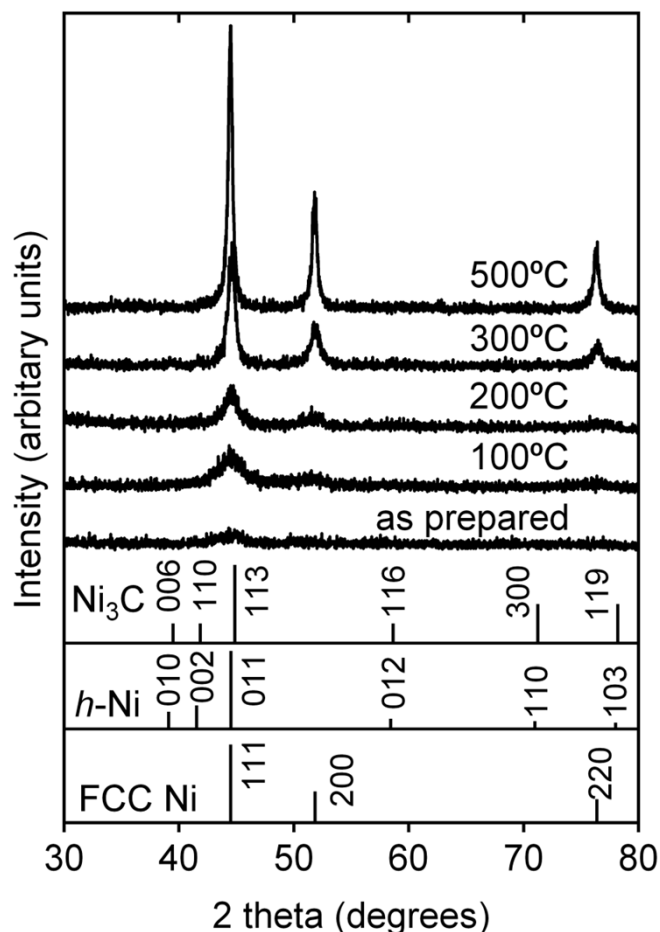


**Figure S9:** *p*XRD profiles for Ni Nps synthesized from Ni(acac)<sub>2</sub>. Simulated *p*XRD peaks for the FCC-type Ni, hcp-type Ni (*h*-Ni), and Ni<sub>3</sub>C are indicated by solid markers at the bottom.

Figure S9 shows the *p*XRD patterns of Ni Nps prepared from Ni(acac)<sub>2</sub> and subsequently annealed in vacuum at different temperatures. The *p*XRD profile for as-prepared Ni Nps shows a broad peak at 45 degrees, corresponding to the 111 reflection of FCC-type Ni (*Fmm*,  $a = 0.3524$  nm; see the simulated *p*XRD pattern at the bottom). At 100 °C, two peaks became visible at 51.84 and 76.38 degrees, corresponding to the 200- and 220 reflections of FCC-type Ni, respectively. The peaks became strong and sharp at elevated temperatures due to particle growth, but there was no sign of the other phase than FCC-type Ni. The approximate particle size of Ni Nps was calculated using Scherrer's equation as 3, 4,

5, 11 and 13 nm for as-prepared, 100 °C-, 200 °C-, 300 °C- and 500 °C-annealed samples, respectively.

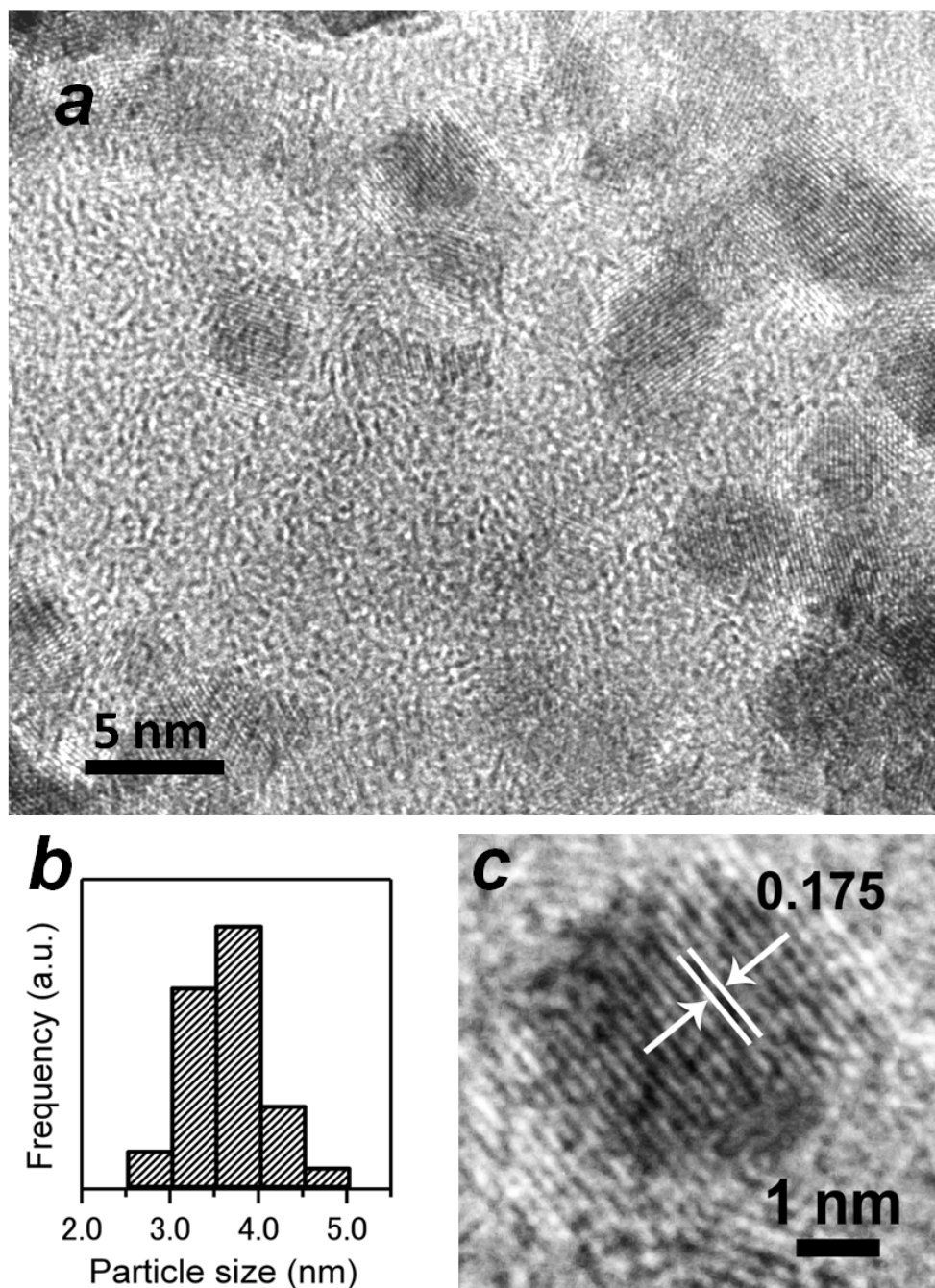


**Figure S10:** (a) Bright-field TEM image, (b) size distribution and (c) high-resolution TEM image of pure Ni NPs.

Figure S10 shows the UHV-TEM images of as-prepared Ni Nps. As expected from

*p*XRD, Ni Nps were ranging in size from 2 to 4.5 nm (average size = 3 nm). Clear lattice fringes were observed over as-prepared Ni Nps, showing that the material was atomically ordered in the FCC-type structure. The interval of the lattice fringe, 0.175 nm, was consistent with the *d*-value for the Ni (200) plane ( $d_{200} = 0.1762$  nm).

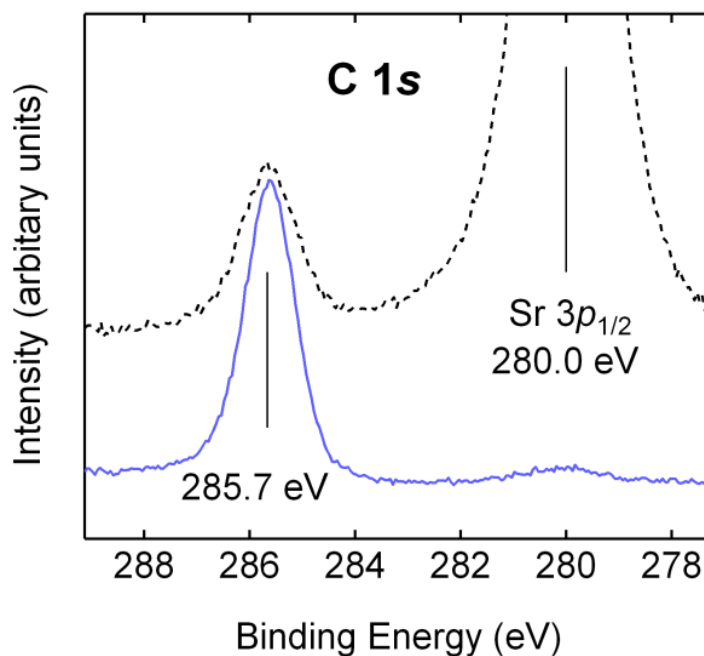


**Figure S11:** HX-PES profiles in the C 1s and Sr 3p<sub>1/2</sub> regions for as-prepared Ni Nps and the SrTiO<sub>3</sub> substrate.

Figure S11 shows the HX-PES profile of as-prepared Ni Nps in the C 1s and Sr 3p<sub>1/2</sub> regions. The C 1s photoemission peak was observed at 285.7±0.2 eV on both Ni Nps and the substrate surface, corresponding to surface contamination. There was no peak in the vicinity of the binding energy of the C 1s peak for Ni<sub>3</sub>C Nps, 283.7±0.2 eV, showing that as-prepared Ni Nps were pure-phased Ni containing no carbides.

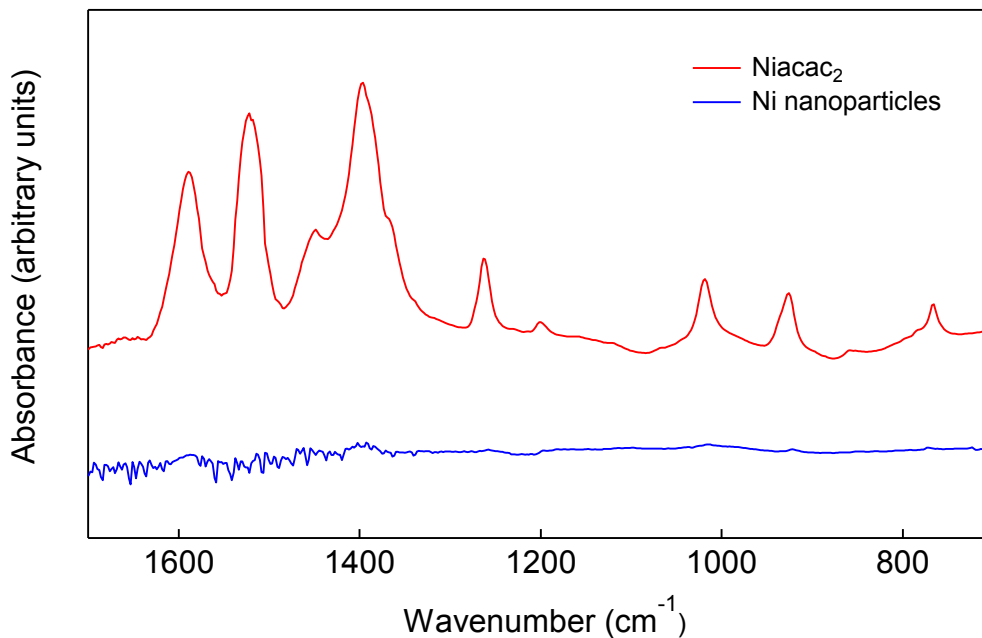


**Figure S12:** FTIR spectra of Niacac<sub>2</sub> (red) and pure Ni Nps (blue).

Figure S12 shows the FTIR spectra of Niacac<sub>2</sub> and as-prepared Ni Nps. All the FTIR peaks corresponding to the vibration of the organic ligand, acetylacetonate (*acac*), became invisible when Niacac<sub>2</sub> was reduced by NaNaph to Ni Nps. The surface of as-prepared Ni Nps was free from organic byproducts.

#### 4. Additional electrochemical data

##### 4.1 NaBH<sub>4</sub> oxidation over Au Nps

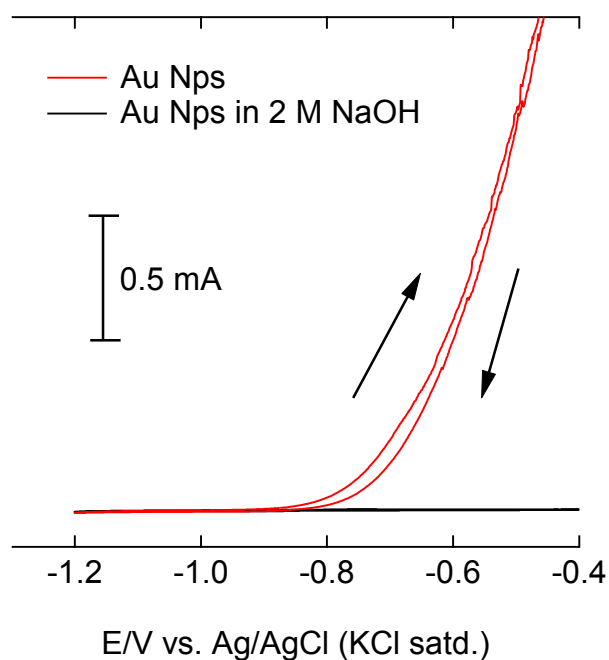


**Figure S13:** CV curves for the NaBH<sub>4</sub>-oxidation reaction over Au Nps.

Figure S13 presents the CV curve for the electrooxidation of NaBH<sub>4</sub> over Au Nps. The anodic wave showed a deviation at an onset potential of -0.86 V from the background CV profile (black curve), obtained in a 2 M NaOH solution containing no fuel.

## 4.2 Methanol oxidation

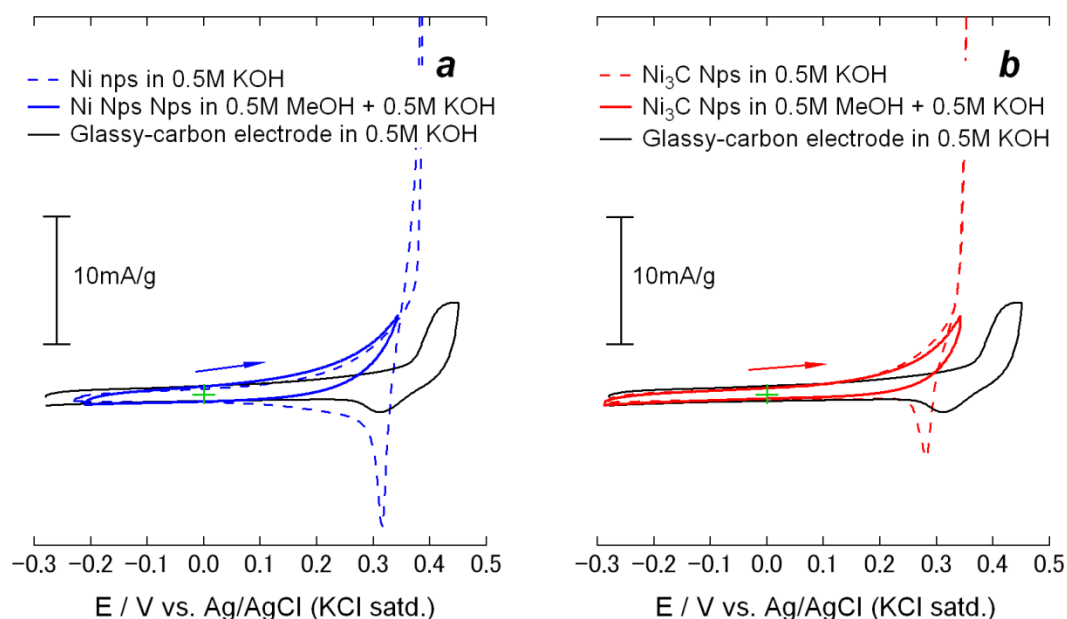


**Figure S14:** CV curves for the methanol-oxidation reactions over (a) Ni Nps and (b) Ni<sub>3</sub>C Nps.

Figure S14a shows the CV curve for the electrooxidation of methanol over Ni Nps. On the anodic sweep from -0.3 to +0.5 V, the CV curve for Ni Nps in a fuel-containing solution (solid blue curve) exhibited a similar onset potential (+0.14 V) than the blank CV curve (+0.15 V; broken blue curve). Figure S14b shows the CV curve for the electrooxidation of methanol over Ni<sub>3</sub>C Nps. On the anodic sweep from -0.3 to +0.5 V, the CV curve for Ni<sub>3</sub>C Nps in a fuel-containing solution (solid red curve) exhibited a very similar onset potential (+0.15 V) as the blank CV curve (+0.15 V; broken red curve). Neither Ni Nps nor Ni<sub>3</sub>C Nps were active toward the electrooxidation of methanol.

## 5. References

1. É. Bencze, B. V. Lokshin, J. Mink, W. A. Herrmann and F. E. Kühn, *J. Organomet. Chem.* 2001, **627**, 55.
2. Z. L. Schaefer, K. M. Weeber, R. Misra, P. Schiffer and R. E. Schaak, *Chem. Mat.* 2011, **23**, 2475.